Communication

Quantum Yield Heterogeneities of Aqueous Single-Wall Carbon Nanotube Suspensions

Jared Crochet, Michael Clemens, and Tobias Hertel

J. Am. Chem. Soc., **2007**, 129 (26), 8058-8059• DOI: 10.1021/ja071553d • Publication Date (Web): 07 June 2007

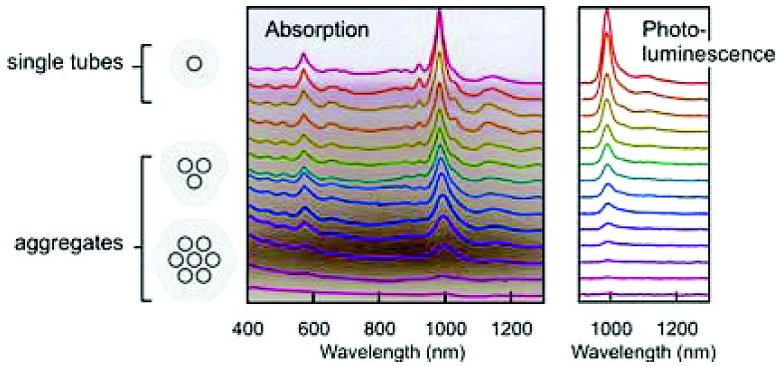

More About This Article

Additional resources and features associated with this article are available within the HTML version:

- Supporting Information
- Links to the 28 articles that cite this article, as of the time of this article download
- Access to high resolution figures
- Links to articles and content related to this article
- Copyright permission to reproduce figures and/or text from this article

View the Full Text HTML

J|A|C|S
COMMUNICATIONS

Published on Web 06/07/2007

Quantum Yield Heterogeneities of Aqueous Single-Wall Carbon Nanotube Suspensions

Jared Crochet,[†] Michael Clemens,[‡] and Tobias Hertel*[,†,§]

Department of Physics and Astronomy, Vanderbilt University, Nashville, Tennessee 37235, Department of Physics and Astronomy, Brigham Young University, Provo, Utah 84602, and Vanderbilt Institute of Nanoscale Science and Engineering, Vanderbilt University, Nashville, Tennessee 37235

Received March 5, 2007; E-mail: tobias.hertel@vanderbilt.edu

Colloidal suspensions provide an ideal platform for spectroscopic studies of vapor phase synthesized, but hydrophobic and practically insoluble, single-wall carbon nanotubes (SWNT). These molecules can be thought of as being rolled up from a slice of a graphene sheet.[1] Their electronic and geometrical structure is uniquely defined by their chiral vector $\boldsymbol{c} = n\boldsymbol{a} + m\boldsymbol{a}_2$, with $\boldsymbol{a}_1$ and $\boldsymbol{a}_2$ being vectors describing the graphene unit cell. SWNTs whose chiral indices (n,m) are related by $(n - m)\mathrm{mod}(3) = \pm 1$ have a direct band gap, and their fluorescence is studied in this communication. Commonly, colloidal nanotube suspensions are prepared by sonication of raw nanotube soot in water with amphiphilic surfactants such as sodium cholate (SC), sodium dodecyl sulfate (SDS), or DNA.[1,2] The resulting dark heterogeneous mixture is ultracentrifuged in order to remove denser nanotube aggregates, catalyst particles, and other carbonaceous constituents. The homogeneous supernatant of these mixtures has been reported to exhibit photoluminescence (PL) quantum yields (QY) η between 10^{-3} and 1.7×10^{-4}.[1,3] Several extrinsic factors such as temperature, inhomogeneities, and tube length for example[4−6] have been identified to influence nonradiative decay, but the magnitude of intrinsic PL quantum yields remains subject to debate. Some recent single tube PL studies, for example, report yields from 10^{-4} to as much as 0.07.[5,7] Here, we report on an optical study of isopycnically fractionated colloidal SWNT suspensions. We find that the most buoyant fractions—which consist of isolated micellar SWNTs—have significantly higher PL QYs than the heterogeneous supernatant of traditionally prepared suspensions. The latter has previously been used for the determination of the ensemble PL QYs cited above. The experiments show that intrinsic PL QYs of SWNTs exceed 1% and are thus significantly larger than previously believed.

SWNT material grown by the CoMoCAT method[8] is dispersed in H_2O with 2 wt % SC by ultrasonication using a Branson 450 horn sonifer. The resulting mixture is centrifuged for 4 h at 31 krpm in a Sorvall ultracentrifuge with a swinging bucket rotor (Sorvall TV-640). The top 50% of the supernatant is decanted and spectroscopically analyzed. Density differentiation of this supernatant is carried out following the procedure outlined by Arnold et al.[9] To this end, we prepare a step gradient consisting of four sections with 2 wt % SC in water containing 18, 13.5, 9, and 0% iodixanol, respectively (Sigma-Aldrich Optiprep). The supernatant is layered into the 13.5% iodixanol fraction (Figure 1a). The centrifuge vial with the step gradient and supernatant is capped and tilted horizontally for 2 h in order to allow for some diffuse mixing of the different sections prior to ultracentrifugation. The same procedure is carried out with a reference sample not containing any CNTs. Both vials are then centrifuged at 41 krpm until visible

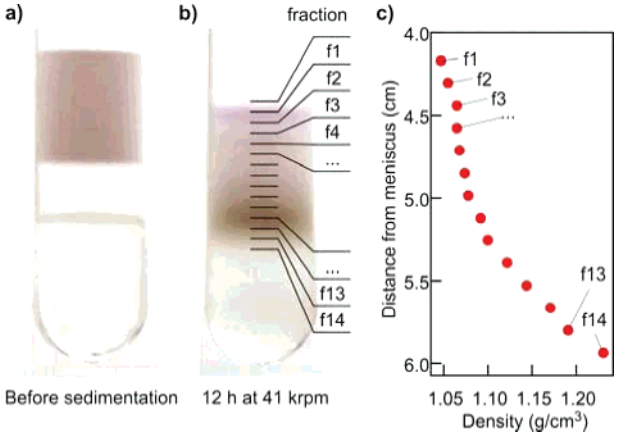

Figure 1. (a) Centrifuge vial with step gradient and a layer of conventionally prepared SWNT suspension. (b) The same vial after ultracentrifugation for 12 h. (c) Measured density profile of the extracted 200 μL fractions after ultracentrifugation.

colored bands appear in the sample vial after 12 h signifying structural separation. Longer centrifugation times do not lead to any significant change of the structure of these bands. The vials are then removed from the centrifuge and are split into fourteen 200 μL fractions by a home-built upward displacement fractionator using Fluorinert FC-40 as a high-density chase medium. The density of fractions in the range of the bands is found to increase from 1.047 to 1.231 g·cm^{-3} (Figure 1c). The density of the purple band with its high concentration of individual (6,5) tubes is (1.055 ± 0.005) g·cm^{-3}.

The fractions are spectroscopically characterized with a Varian Cary 5000 UV−vis−NIR spectrophotometer and a Jobin Yvon/Horiba Fluorolog-3 FL3-111 spectrophotofluorometer equipped with a liquid nitrogen cooled InGaAs detector. Solvent background correction is facilitated using fractions drawn in identical intervals from the reference vial.

Absorption spectra from the topmost fractions in Figure 2a are characterized by a low nonresonant background and a strong absorption signal at 981 nm. A spectrum of the unfractionated supernatant from the starting material is also included in Figure 2a for comparison (dashed line). The 981 nm feature is associated with the first subband E_{11} exciton transition in the (6,5) tube, which is here estimated to account for about 40% of the absorption signal by semiconducting tubes in the 800−1250 nm range. The other most dominant and partially overlapping absorption features in this frequency range are those of the (6,4) at 882 nm, (9,1) at 922 nm, (8,3) at 963 nm, (7,3) at 998 nm, and (7,5) at 1022 nm, as well as features in a more strongly congested region around 1150 nm. The purple coloration of the topmost band can be attributed to the energetic position of the higher lying E_{22} subband exciton which,

[†] Department of Physics and Astronomy, Vanderbilt University.
[‡] Brigham Young University.
[§] Vanderbilt Institute of Nanoscale Science and Engineering, Vanderbilt University.

10.1021/ja071553d CCC: $37.00

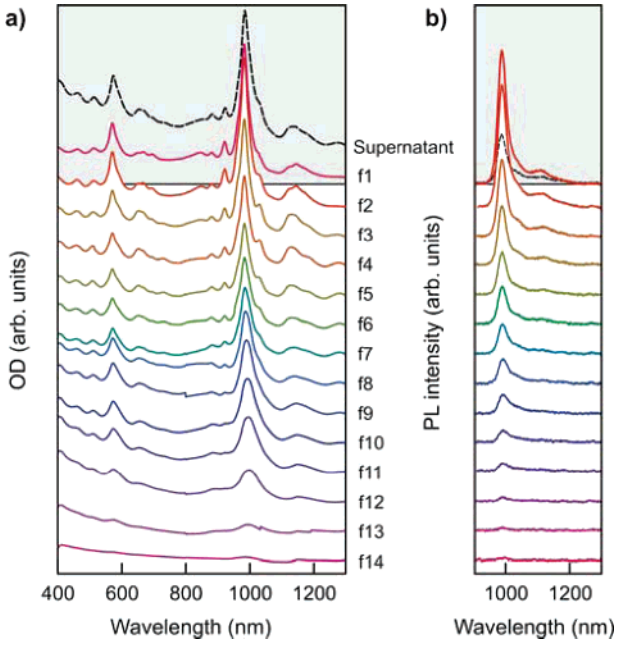

Figure 2. (a) Absorption spectra of fractions f1−f14 as drawn from the vial in Figure 1b. Spectra of the supernatant are shown as dashed lines to scale with fraction f1 where the lower boundary of the gray box signifies the respective zero lines. (b) Photoluminescence spectra from the same fractions for excitation at 571 nm.

for the dominant (6,5) tube, lies at 571 nm. The higher nonresonant background in the visible spectrum of the supernatant is what gives rise to the gray discoloration of the starting material despite similarly enhanced absorption at 571 nm.

Spectra from fractions f3−f6 are characterized by a continuous shift of spectral weight from the (6,5) tube to tubes with lager diameter indicative of increasing tube density with diameter with a slope of 120 000 g·cm^{-4}, similarly to DNA stabilized suspensions.[9] The diameter dependence of the density of SC suspended SWNTs is obtained from a similar series of absorption spectra from more polydisperse CoMoCAT starting material (see Supporting Information). Fractions following f6 exhibit increasingly broadened absorption features indicative of the formation of aggregates and small nanotube bundles.[9] Absorption features in colloidal SWNT suspensions, for example, are blue shifted by 50 meV with respect to similar features observed for nanotube ropes.[10] The PL spectra for excitation at 571 nm shown in Figure 2b, on the other hand, exhibit a continuous decrease of the PL intensity from the topmost fractions down to the densest fractions which do not photoluminesce. The sum of all absorption and emission spectra is found to exactly match the respective spectra from the supernatant starting material (see Supporting Information).

If the optical density at 571 nm and the spectrally integrated PL intensity are compared, we find that the PL quantum yield decreases monotonically from f1 to f14 (Figure 3). Absolute PL quantum yields η are obtained by comparison with a reference dye, Styryl 13 (Radiant Dyes Laser & Accessories GmbH, laser dye LDS 925) with 11% QY. Details on the procedure used here for determination of PL quantum yields from a reference are discussed in the Supporting Information as well as in ref 11. The absorption maximum of the reference dye at 580 nm and its emission maximum at 960 nm are a nearly perfect match with the E_{22} absorption and E_{11} emission lines of the (6,5) tube, which helps to reduce inherent uncertainties in the determination of PL QYs by comparison with a reference. The absolute PL quantum yield of fraction f1 of (1.1 ± 0.1)% is found to be over a factor of 5 higher than that of the

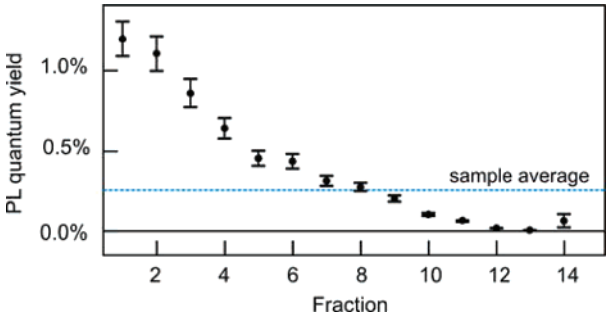

Figure 3. Photoluminescence quantum yield for each of the 14 measured fractions. The PL QY of the topmost purple fractions is found to be over a factor of 5 higher than that of the supernatant or average over all fractions.

supernatant or ensemble average. This value also significantly exceeds previous ensemble estimates of 10^{-3} or 1.7×10^{-4} by over an order of magnitude.[1,3]

The decrease of PL quantum yields with sample density is most likely associated with the presence of small nanotube aggregates and bundles in the denser fractions. The broadening of spectral features and a slight red shift of absorption and emission lines both indicate that the dielectric environment changes slightly in the denser fractions. Bundling is predicted to be accompanied by a small increase of the dielectric function which should lead to the observed red shifts.[12] The decreasing PL QY could then be related to energy transfer from the semiconducting nanotubes to residual metallic tubes and successive nonradiative decay within the metallic species. These findings also have far reaching consequences for the interpretation of a host of experiments on conventionally prepared nanotube suspensions, which are here found to be very heterogeneous with respect to their composition, containing not only individual tubes but at least $^2/_3$ of aggregates with small admixtures of metallic tubes. A recent study moreover suggests that length selection of longer tubes may increase the PL QYs possibly by as much as another factor of 5.[6] This would, for the first time, bring ensemble quantum yields in line with recent spectacular estimates of single tube PL QYs on the order of 7%.[7]

Acknowledgment. This work is supported through an ACS grant (PRF 44479-AC10) as well as by the NSF through an IGERT grant (DGE 0333392). We also thank Michael S. Arnold for numerous helpful discussions.

Supporting Information Available: Additional experimental details. This material is available free of charge via the Internet at http://pubs.acs.org.

References

(1) O'Connell, M. J.; Bachilo, S. M.; Huffman, C. B.; Moore, V. C.; Strano, M. S.; Haroz, E. H.; Rialon, K. L.; Boul, P. J.; Noon, W. H.; Kittrell, C.; Ma, J. P.; Hauge, R. H.; Weisman, R. B.; Smalley, R. E. *Science* **2002**, *297*, 593−596.
(2) Weisman, R. B.; Bachilo, S. M. *Nano Lett.* **2003**, *3*, 1235−1238.
(3) Wang, F.; Dukovic, G.; Brus, L. E.; Heinz, T. F. *Phys. Rev. Lett.* **2004**, *92*, 177401−177404.
(4) Mortimer, I. B.; Nicholas, R. J. *Phys. Rev. Lett.* **2007**, *98*, 27404−27408.
(5) Hagen, A.; Steiner, M.; Raschke, M. B.; Lienau, C.; Hertel, T.; Qian, H. H.; Meixner, A. J.; Hartschuh, A. *Phys. Rev. Lett* **2005**, *95*, 197401−197404.
(6) Heller, D. A.; Mayrhofer, R. M.; Baik, S.; Grinkova, Y. V.; Usrey, M. L.; Strano, M. S. *J. Am. Chem. Soc.* **2004**, *126*, 14567−14573.
(7) Lefebvre, J.; Austing, D. G.; Bond, J.; Finnie, P. *Nano Lett.* **2006**, *6*, 1603−1608.
(8) Kitiyanan, B.; Alvarez, W. E.; Harwell, J. H.; Resasco, D. E. *Chem. Phys. Lett.* **2000**, *317*, 497−503.
(9) Arnold, M. S.; Stupp, S. I.; Hersam, M. C. *Nano Lett.* **2005**, *5*, 713−718.
(10) Hagen, A.; Hertel, T. *Nano Lett.* **2003**, *3*, 383−388.
(11) Williams, A. T. R.; Winfield, S. A.; Miller, J. N. *Analyst* **1983**, *108*, 1067−1071.
(12) Ando, T. *J. Phys. Soc. Jpn.* **1997**, *66*, 1066−1073.

JA071553D